Journal of Applied Fluid Mechanics, Vol. 10, No. 4, pp. 1113-1124, 2017.
Available online at www.jafmonline.net, ISSN 1735-3572, EISSN 1735-3645.
DOI: 10.18869/acadpub.jafm.73.241.27297

Combined Solutal and Thermal Buoyancy Thermocapillary Convection in a Square Open Cavity

A. Alhashash[1] and H. Saleh[2†]

[1] *Science Department, Al-Jouf University, 24241 Sakaka Aljawf, Saudi Arabia*
[2] *Department of Mathematics, University of Riau, 28293 Pekanbaru, Indonesia*

†*Corresponding Author Email: dr.habibissaleh@gmail.com*

(Received October 19, 2016; accepted February 16, 2017)

ABSTRACT

Combined solutal and thermal buoyancy–thermocapillary convection in a square open cavity is studied numerically in the present article. The Forchheimer–Brinkman-extended Darcy model is used in the mathematical formulation for the porous layer and the COMSOL Multiphysics software is applied to solve the dimensionless governing equations. The governing parameters considered are the thermal Marangoni number, $-1000 \le Ma\_T \le 1000$, the Darcy number, $10-5 \le Da \le 10-2$, the porosity of porous medium, $0.4 \le \varepsilon \le 0.99$ and the Lewis number, $10 \le Le \le 200$. It is found that the global heat and solute transfer rate decreases by reducing the counteracting surface tension force and increases by augmenting the surface tension force. The minimum values of the global heat and solute transfer rate were obtained about $Ma\_T = -90$ for the all porosities.

Keywords: Marangoni convection; Natural convection; Porous cavity; Forchheimer brinkman model.

NOMENCLATURE

C,S	concentration, dimensionless concentration	α	effective thermal diffusivity
D	species diffusivity	β_C	thermal expansion coefficient for concentration
Da	Darcy number	β_T	thermal expansion coefficient for temperature
F	inertia coefficient	γ_C	solutal surface tension gradient
g	gravitational acceleration	γ_T	thermal surface tension gradient
K	permeability of the porous medium	ℓ	width and height of cavity
Le	Lewis number	ε	porosity
Ma	Marangoni number	Θ	dimensionless temperature
N	kinematic viscosity	**Subscript**	
N	buoyancy ratio	C	cold
Nu	Nusselt number	f	fluid
Pr	Prandtl number	h	hot
Ra	Rayleigh number	0	reference value
Sh	Sherwood number		

1. INTRODUCTION

Natural convection due to combined buoyancy effect of thermal and species diffusion in a fluid saturated porous medium has received considerable attention in the last two decades owing to its applications. The phenomenon of the combined buoyancy effect is usually referred to as double diffusive convection. The theoretical work for double diffusive convection in a porous cavity has been pioneered by Nithiarasu *et al*. (1985), Mamou *et al*. (1995). They applied Darcy models for the porous layer. Goyeau *et al*. (1996), Nithiarasu *et al*. (1996), Karimi-Fard *et al*. (1997) applied non-Darcy models for the porous layer. Chamkha (2002) included the heat generation and absorption effects in the porous cavity. He concluded that the average Nusselt and Sherwood numbers decrease as a result of heat generation and increase as a result of heat absorption. Liu *et al*. (2008) included the solute sources and Tofaneli and

de Lemos (2009) considered the turbulent natural convection. Al-Farhany and Turan (2012) showed that the average Nusselt and Sherwood numbers decrease when the inclination angle of the cavity increases. Benissaad and Ouazaa (2012) used the model of Darcy and a porous medium saturated by a binary fluid. An excellent agreement between the analytical solution and the numerical simulation were obtained. Hadidi *et al*. (2016) considered the heat and mass transfer generated horizontal partially porous enclosure. Recently, Ghalambaz *et al*. (2016) investigated natural convection and two different chemical components have dissolved in the fluid saturated porous medium which have separate concentrations.

Double diffusive and Marangoni convection in a cavity filled with viscous fluid was studied by Arafune and Hirata (1998). They found the concentration field changes by the existence of solutal Marangoni convection. Jue (1998) considered the similar configuration and found the Marangoni effect enhances or decreases the circulation strength. Marangoni convection occurs when the surface tension of an interface (generally liquid-air) depends on the concentration of a species or on the temperature. Marangoni convection may be called thermocapillary convection. Previously, the theoretical work for natural and Marangoni convection has been pioneered by Strani *et al*. (1983). They concluded that the surface deformation had a negligible influence on the qualitative aspects of the flow-field structure at low crispation number. Srinivasan and Basu (1986) found that buoyancy driven flow has been shown to be negligible compared to surface tension gradient driven flow in laser melting. Bergman and Ramadhyani (1986) investigated numerically the characteristics of buoyancy driven flow in a square cavity. They showed that surface tension significantly alters the buoyant flow. The boundary layer scalings for buoyant and thermocapillary convection have been established well Carpenter and Homsy (1989). Then, Hadid and Roux (1992) analyzed a shallow cavity and showed that surface tension can have a quite significant effect on the stability of a primary buoyancy driven flow. Effects of a magnetic field on the combined convection were studied by Rudraiah *et al*. (1995) and Hossain *et al*. (2005). Saleem *et al*. (2011) examined a square cavity whose right wall is kept open for flow entrainment and exit. Recently, Arbin *et al*. (2016) reported the effect of the Marangoni number, Lewis number and heater size on the contours of streamlines, isotherms, isoconcentrations, masslines and heatlines in an open top square cavity with partially heated and salted from the side.

In this paper, double diffusive–thermocapillary convection in a square cavity is investigated. The convective flows induced by the combined action of both temperature and solutal gradients in porous media has surged in view of its importance in many engineering problems, such as migration of moisture contained in fibrous insulation, grain storage, the underground disposal of nuclear wastes, and drying processes in the top-free cavity, especially under a small-scale system or under low-gravity hydrodynamics environment. The non-Darcy model is used for the porous layer. Two opposing walls of the cavity are maintained at fixed but different temperatures and concentrations, while the other two walls are adiabatic. The results are presented in term of stream functions, isotherms, isoconcentration lines and Nusselt and Sherwood number.

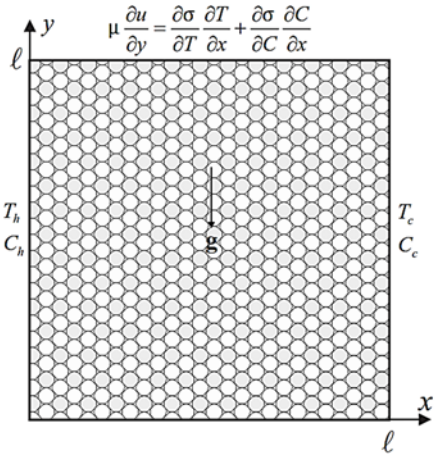

a

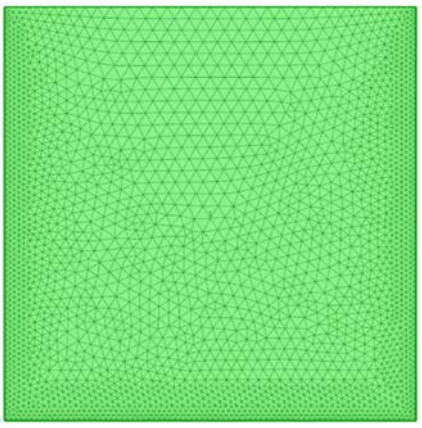

b

Fig. 1. (a) Schematic representation of the model, (b) Mesh distribution.

2. MATHEMATICAL FORMULATION

Consider a square cavity as shown in Fig. 1. The left wall is kept at high temperature (T_h) and high concentration (C_h), the right wall at low temperature (T_c) and low concentration (C_c) and the bottom and top walls are adiabatic. The top free surface is assumed to be flat and non–deformable which corresponds to a situation with very high surface tension. The surface tension, σ, on the upper boundary is assumed to vary linearly with temperature and concentration gradients as:

$$\sigma=\sigma_0[1-\gamma_T(T-T_0)-\gamma_C(C-C_0)] \quad (1)$$

where $T_0=(T_h+T_c)/2$ is the mean temperature, $C_0=(C_h+C_c)/2$ is the mean mass fraction, $\gamma=(1/\sigma_0)(\partial\sigma/\partial T)$ is the temperature coefficient of the surface tension, σ0 is a reference surface tension. The fluid is assumed to be Newtonian and incompressible. The flow is steady and laminar and further we assume that there is no internal heat generation, absorption,

Soret, Dufour or viscous dissipation. No–slip conditions are applied on all boundaries, except the case where the upper free surface relates the velocity gradient to the temperature gradient. Finally, the direction of the gravitational force is in the negative y-direction. Under the above assumptions, the conservation equations for mass, momentum and energy in a two–dimensional Cartesian co–ordinate system are (Hossain *et al*. (2005)):

$$\frac{\partial u}{\partial x}+\frac{\partial v}{\partial y}=0$$

$$\frac{u}{\varepsilon^2}\frac{\partial u}{\partial x}+\frac{v}{\varepsilon^2}\frac{\partial u}{\partial y}=-\frac{1}{\rho_f}\frac{\partial p}{\partial x}+\frac{\mu}{\varepsilon\rho_f}\left(\frac{\partial^2 u}{\partial x^2}+\frac{\partial^2 u}{\partial y^2}\right) \quad (2)$$

$$-\frac{\mu}{K}u-F\rho_f\frac{\sqrt{u^2+v^2}}{\sqrt{K}}u \quad (3)$$

$$\frac{u}{\varepsilon^2}\frac{\partial v}{\partial x}+\frac{v}{\varepsilon^2}\frac{\partial v}{\partial y}=-\frac{1}{\rho_f}\frac{\partial p}{\partial y}+\frac{\mu}{\varepsilon\rho_f}\left(\frac{\partial^2 v}{\partial x^2}+\frac{\partial^2 v}{\partial y^2}\right)$$
$$-\frac{\mu}{K}u-F\rho_f\frac{\sqrt{u^2+v^2}}{\sqrt{K}}v$$
$$+\beta_T g(T-T_0)+\beta_C g(C-C_0) \quad (4)$$

$$u\frac{\partial T}{\partial x}+v\frac{\partial T}{\partial y}=\alpha\left(\frac{\partial^2 T}{\partial x^2}+\frac{\partial^2 T}{\partial y^2}\right) \quad (5)$$

$$u\frac{\partial C}{\partial x}+v\frac{\partial C}{\partial y}=D\left(\frac{\partial^2 C}{\partial x^2}+\frac{\partial^2 C}{\partial y^2}\right) \quad (6)$$

The appropriate boundary conditions are:

$u=v=0,\ C=C_h$ and $T=T_h$ at $x=0$ (7)

$u=v=0,\ C=C_c$ and $T=T$ at $x=\ell_c$ (8)

u=v=0, $\frac{\partial C}{\partial y}=0$ and $\frac{\partial T}{\partial y}=0$ at y=0 (9)

$$\mu\frac{\partial u}{\partial y}=\frac{\partial\sigma}{\partial T}\frac{\partial T}{\partial x}+\frac{\partial\sigma}{\partial C}\frac{\partial C}{\partial x} \quad at \quad y=\ell \quad (10)$$

The dynamic boundary conditions on the top free surface relates the velocity gradient to the temperature gradient and this represents the balance between the shear stress and the surface tension gradient at surface which is responsible for establishment of thermocapillary flow in the cavity.

Equations (2) through (10) can be reduced (after eliminating the pressure gradient terms) and made dimensionless by using the following variables:

$$X=\frac{x}{\ell},\ Y=\frac{y}{\ell},\ U=\frac{u\ell}{\alpha},\ Le=\frac{\alpha/k}{D},$$
$$\Theta=\frac{T-T_c}{T_h-T_c},\ S=\frac{C-C_c}{C_h-C_c},\ Ra_T=\frac{\beta g\Delta T\ell^3}{\nu\alpha},$$
$$Ma_T=\frac{\partial\sigma}{\partial T}\frac{\Delta T}{\mu\alpha}\ Ma_c\frac{\partial\sigma}{\partial C}\frac{\Delta C\ell}{\mu\alpha}$$

$$Da=\frac{K}{\ell^2},\ N=-\left(\frac{\beta c\Delta C}{\beta_T\Delta T}\right) \quad (11)$$

to result the following dimensionless equations:

$$\frac{\partial U}{\partial X}+\frac{\partial V}{\partial Y}=0$$
$$\frac{U}{\varepsilon^2}\frac{\partial U}{\partial X}+\frac{V}{\varepsilon^2}\frac{\partial U}{\partial Y}=\frac{\partial P}{\partial X}-\frac{\Pr}{Da}U \quad (12)$$

$$-F\frac{\sqrt{U^2+V^2}}{\sqrt{Da}}U+\frac{\Pr}{\varepsilon}\left(\frac{\partial^2 U}{\partial X^2}+\frac{\partial^2 U}{\partial Y^2}\right)$$
$$\frac{U}{\varepsilon^2}\frac{\partial V}{\partial X}+\frac{V}{\varepsilon^2}\frac{\partial V}{\partial Y}=-\frac{\partial P}{\partial Y}-\frac{\Pr}{Da}V \quad (13)$$
$$-F\frac{\sqrt{U^2+V^2}}{\sqrt{Da}}V+\frac{\Pr}{\varepsilon}\left(\frac{\partial^2 v}{\partial x^2}+\frac{\partial^2 V}{\partial Y^2}\right)$$

$$+R_{aT}\Pr\ (\Theta\text{-NS}) \quad (14)$$

$$U\frac{\partial\Theta}{\partial X}+V\frac{\partial\Theta}{\partial Y}=\left(\frac{\partial^2\Theta}{\partial X^2}+\frac{\partial^2\Theta}{\partial Y^2}\right) \quad (15)$$

$$U\frac{\partial S}{\partial X}+V\frac{\partial S}{\partial Y}=\frac{1}{Le}\left(\frac{\partial^2 S}{\partial X^2}+\frac{\partial^2 S}{\partial Y^2}\right) \quad (16)$$

to result the following dimensionless equations:

U=V=0, $S=\frac{1}{2},\ \Theta=\frac{1}{2}$ *at* $X=0$ (17)

U=V=0, $S=\frac{-1}{2},\ \Theta=\frac{-1}{2}$ *at* $X=1$ (18)

U=V=0, $\frac{\partial S}{\partial Y}=0$ *and* $\frac{\partial\Theta}{\partial Y}=0$ *at* $Y=0$ (19)

U=V=0, $\frac{\partial S}{\partial Y}=0$ *and* $\frac{\partial\Theta}{\partial Y}=0$ *and*
$$\frac{\partial U}{\partial Y}=Ma_T\frac{\partial\Theta}{\partial X}+Ma_C\frac{\partial S}{\partial X} \quad at \quad Y=1 \quad (20)$$

where F = 1.75/($\sqrt{150}\varepsilon^{3/2}$) is the inertia coefficient according to the Ergun (1952) correlation.

3. NUMERICAL METHOD AND VALIDA TION

The governing equations along with the boundary conditions are solved numerically by the CFD software package COMSOL Multiphysics. COMSOL Multiphysics (formerly FEMLAB) is a finite element analysis, solver and simulation software package for various physics and engineering applications. We consider the following application modes in COMSOL Multiphysics. The Incompressible Laminar Flow Equations mode (spf) for Eqs. (12)–(14), the Heat Transfer Equations mode (ht) for Eq.(15) and the Heat Equations mode (hteq) for Eq.(16). In this study, mesh generation on square cavity is made by using triangles. The triangular mesh distribution is shown in Fig. 1(b). P2-P1 Lagrange

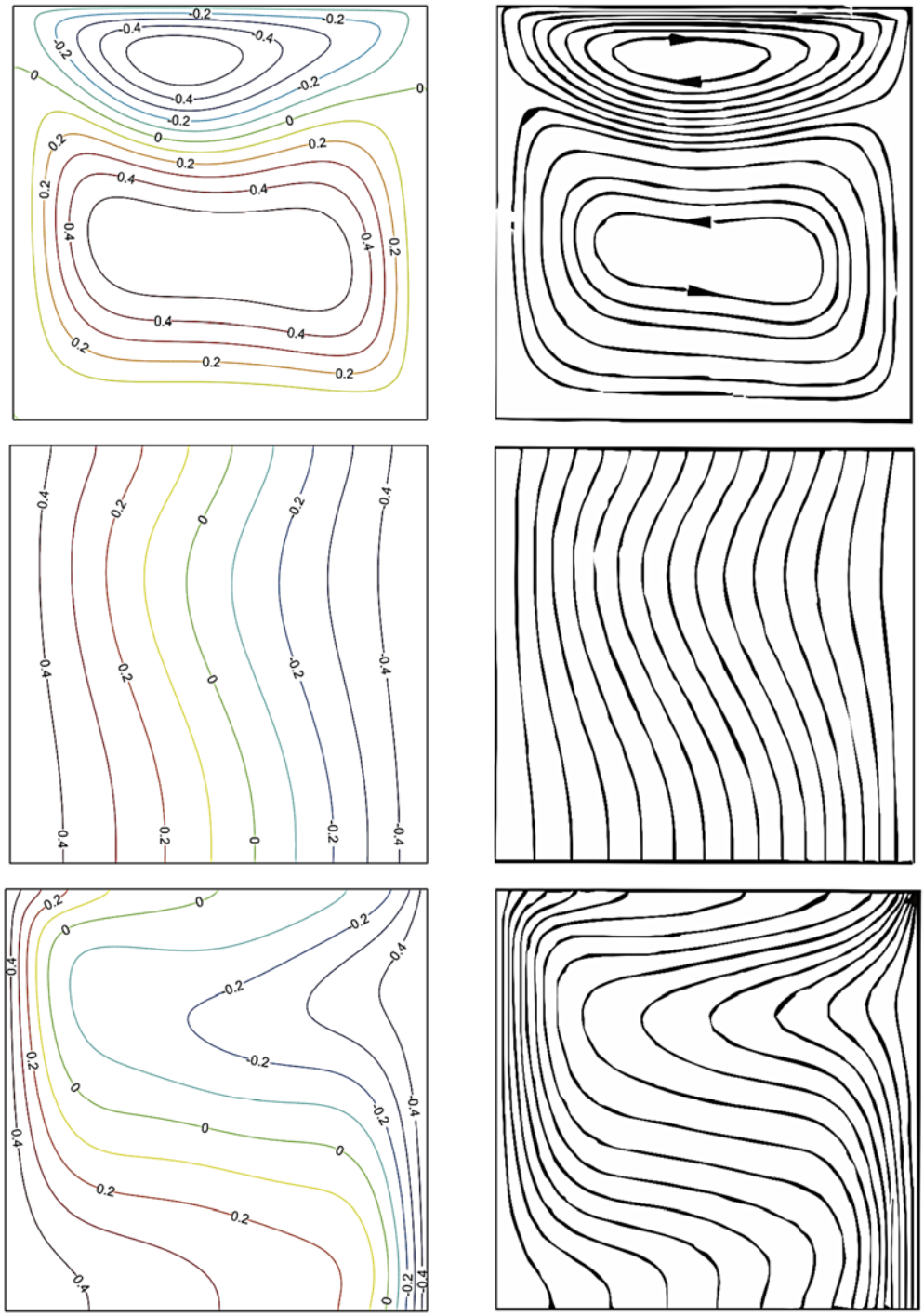

Fig. 2. Comparison of the present computed steady state streamlines, isotherms and isoconcentration (left) against that of literature (right) for a pure fluid, ε=0.99, Da=107, Pr=7.6, N=5, Le=10, $R_{aT}=10^3$, $M_{aT}=M_{aC}=-100$.

elements and the Galerkin least-square method are used to assure stability.

Several grid sensitivity tests were conducted to determine the sufficiency of the mesh scheme and to ensure that the results are grid independent. We use the COMSOL default settings for predefined mesh sizes, i.e. extra coarse, coarser, coarse, normal, fine, finer, extra fine and extremely fine. In the tests, we consider the parameters M_{aT} = 100, N = 5, Pr = 1, Ra = 10^3 and Da = 10−2 as tabulated in Table 1. Considering both accuracy and time, an extra fine mesh size was selected for all the computations done in this paper. As a validation, our results for the isotherms compare well with that obtained by Jue (1998) for a special case, pure fluid, ε = 0.99, Da = 10^7, Pr = 7.6, N = 5, Le = 10, R_{aT} = 103, M_{aT} = M_{aC} = −100 as shown in Fig. 2.

Table 1 Grid sensitivity checks at M_{aT}=100, N=5, Pr=1, Ra=10^3 and Da=10^{-2}

Predefined mesh size	Mesh elements	$\overline{Nu}$	$\overline{Sh}$	CPU time (s)
Extra coarse	286	1.0504	8.3246	3
Coarser	451	1.0340	8.1739	4
Coarse	865	1.0226	7.8188	5
Coarse	1273	1.0173	7.6723	5
Fine	2220	1.0131	7.5209	7
Finer	5577	1.0110	7.2511	12
Extra fine	14105	1.0099	7.1343	28
Extremely fine	23875	1.0092	7.1468	55

4. RESULTS AND DISCUSSION

The analysis in the undergoing numerical investigation are performed in the following range of the associated dimensionless groups: the thermal Marangoni number, $-1000 \le M_{aT} \le 1000$, the Darcy number, $10^{-5} \le Da \le 10^{-2}$, the porosity of porous medium, $0.4 \le \varepsilon \le 0.99$ and the Lewis number, $10 \le Le \le 200$. The buoyancy ratio, Prandtl number and the Rayleigh number are fixed at N = 5, Pr = 1 and Ra = 10^3, respectively. The solutal Marangoni number is considered equal to the thermal Marangoni number for the all figures.

Figure 3(a)-(d) show the effects of M_{aT} on the flow, thermal and concentration fields in the porous cavity with constant values of Le = 10, Da = 10−2 and ε = 0.7. As can be seen in Fig. 3, the ambient fluid interacts with the fluids inside the cavity at upper part the opening and the fluid near the hot wall receives some heat from the heating wall that rise the fluid temperature and concentration. The hot fluid has lower density than the cold fluid. This creates a flow circulation in the cavity, but at a strong, negative thermal Marangoni number (Fig. 3(a)), the flow circulation is driven by surface tension convection. The capillary driven convection is opposite to buoyancy driven convection. The vortex driven by surface tension occupies half of the domain and impels the isoconcentration lines to be denser at the top right comer. The counteracting case displays a decreased value of the absolute Ψmin, and the turning point exists much closer to the top surface for a lower counteracting surface tension force For the M_{aT} = −100, the Marangoni convection flow produces less influence and dominates less area than that of the MaT = −1000 case. This condition does not occur at the augmenting case. The penetration area does not increase prominently by increasing the positive Marangoni number. The strength of the flow circulation increases significantly by increasing the positive Marangoni number (known from Ψmax values). The boomerang shape can not be found here, because the surface tension flow aids the buoyancy flow.

Figure 4(a)-(d) show the effects of Da on the flow, thermal and concentration fields in the porous cavity with constant values of Le = 10, M_{aT} = −100 and ε = 0.7. The intensity of the main flow at the bottom portion due to gravity force weakens by increasing the Darcy number. On the other hand, the intensity of the secondary flow at the top portion due to thermocapillary force strengthens by increasing the Darcy number. The concentration buoyancy convection is greater than the thermal convection in this condition with N = 5 for the all cases. The isotherms and isoconcentration display similar structure at relative low Darcy number. When the Darcy number increases, the flow is fast, Darcys forces are also very large and tend to reduce the velocities at the edge of the solutal boundary layers instantly. Hence, the rest of the cavity is almost stratified. In the stratified areas, the mass transfer is mostly restricted to the diffusive mechanism.

Figure 5(a)-(d) show the effects of Le on the flow, thermal and concentration fields in the porous cavity with constant values of Da = 10^{-2}, M_{aT} =−100 and ε = 0.7. The thermosolutal convection weakens and Marangoni convection strengthens by increasing Lewis number. When the Lewis number increases, the thickness of the boundary layer decreases, and hence, the buoyancy force due to mass transfer could be distributed in a narrow area; as a result, the induced velocities in the cavity are coarse.

Figure 6 (a) illustrates the variation of average Nusselt number along the hot and cold walls versus Darcy number for ε = 0.7 and MaT = −100 at different values of Lewis number. It is noticed that the average Nusselt number values are increased exponentially for the for the all values of Lewis number. The increased Darcy number leads to enhanced fluid movement. The existence

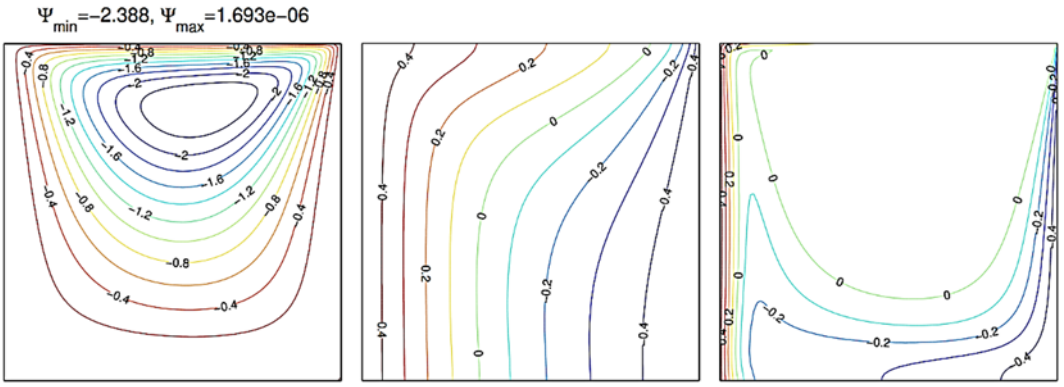

(a) $M_{aT} = -1000$

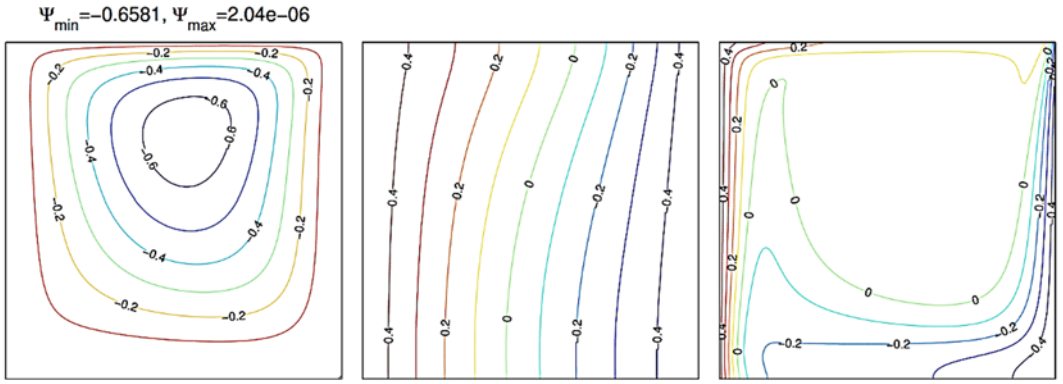

(b) $M_{aT} = -100$

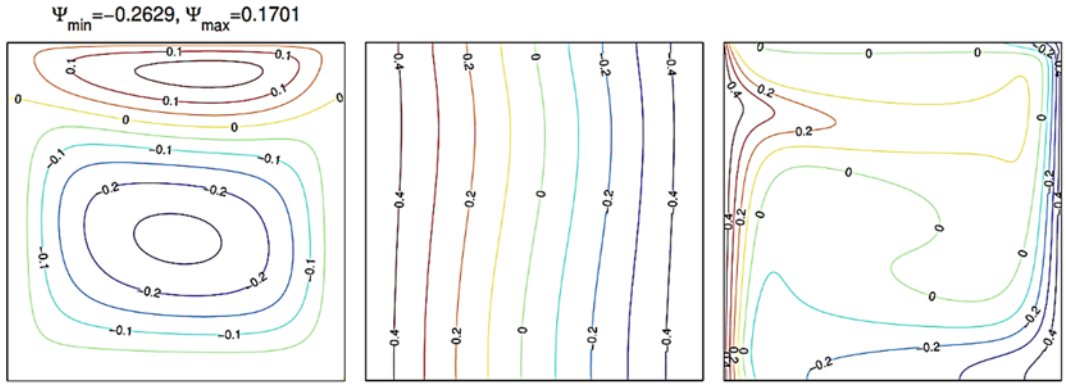

(c) $M_{aT} = 100$

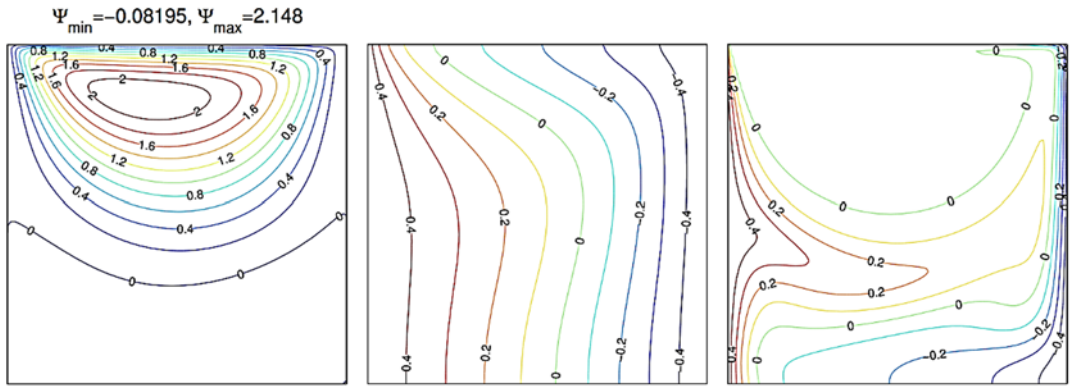

(d) MaT = 1000

Fig. 3. Streamlines (left), isotherms (middle) and isoconcentrations (right) evolutions by varying thermal Marangoni number for $Le=10$, $Da=10^{-2}$ and $\epsilon=0.7$.

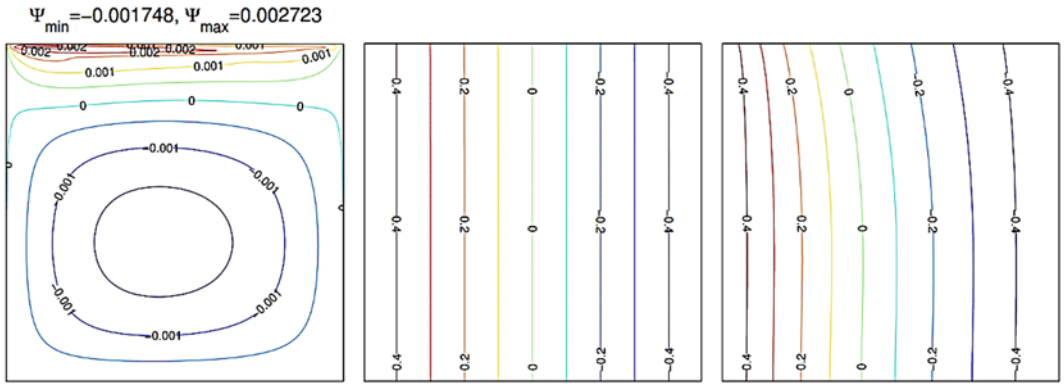

(a) Da = 10^{-5}

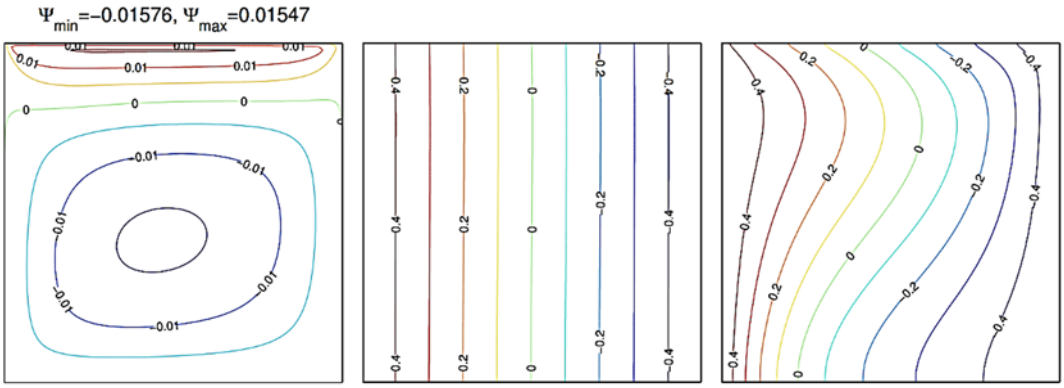

(b) Da = 10^{-4}

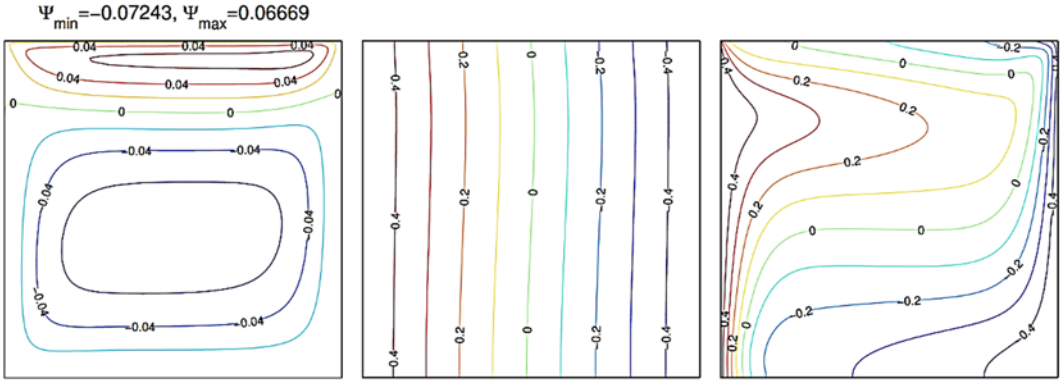

(c) Da = 10^{-3}

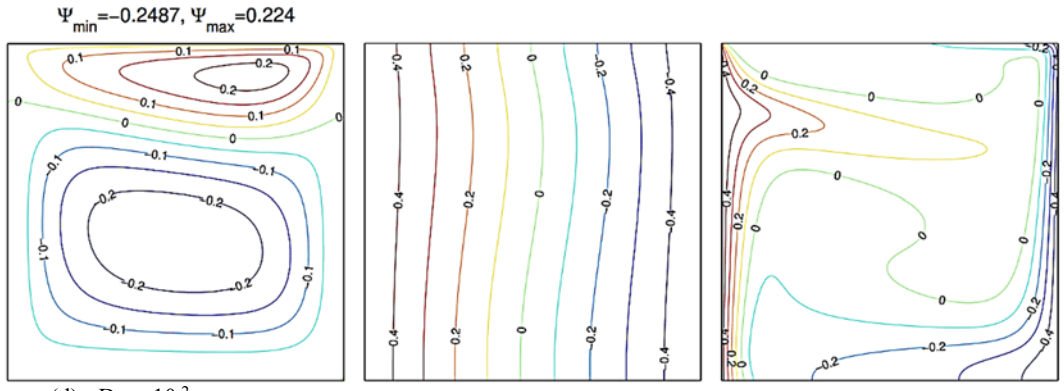

(d) Da = 10^{-2}

(e) Fig. 4. Streamlines (left), isotherms (middle) and isoconcentrations (right) evolutions by varying the Darcy number for Le=10, M_{aT}=−100 and ε=0.7.

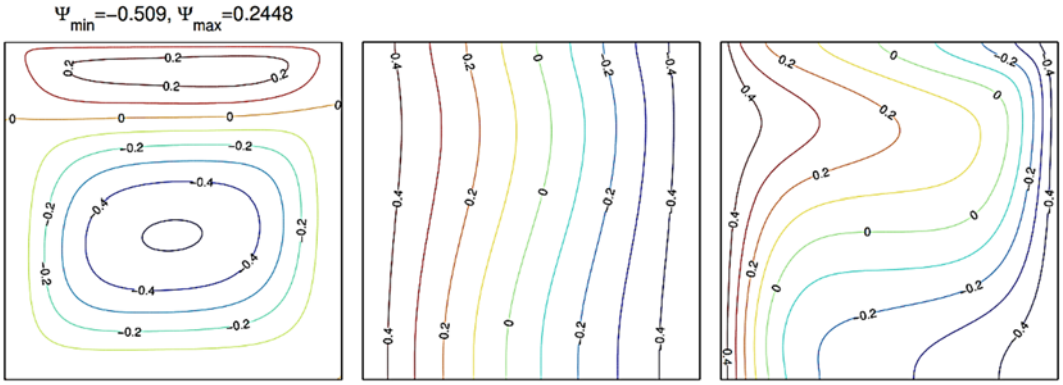

(a) Le = 10

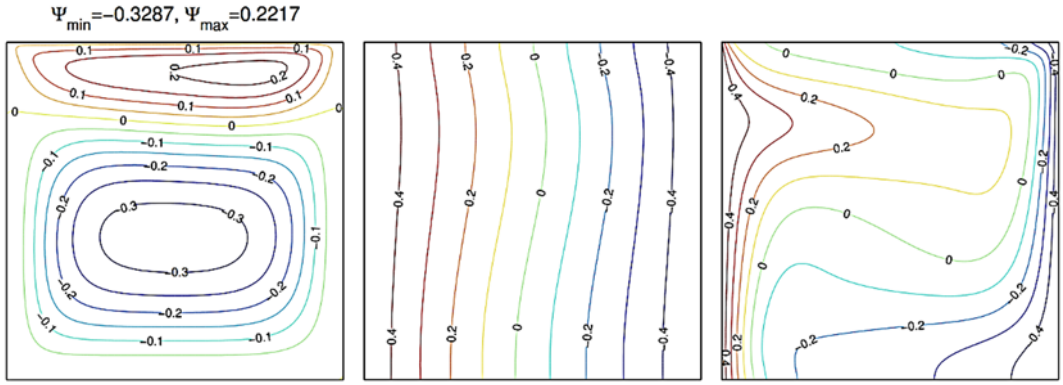

(b) Le = 30

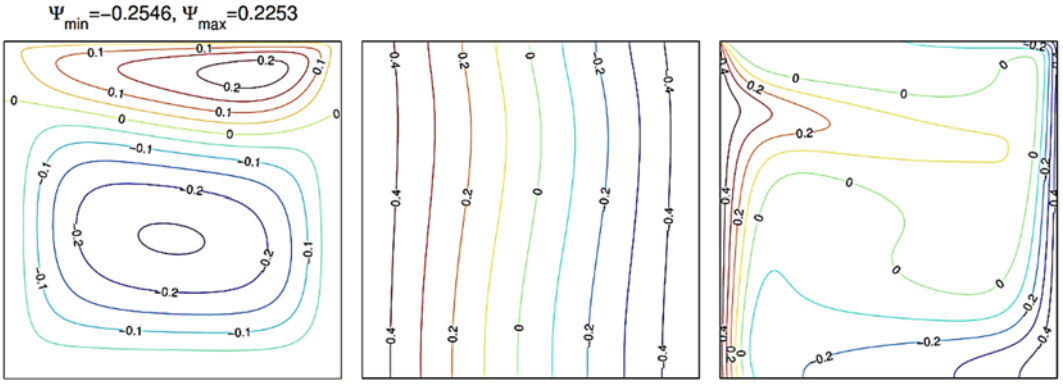

(c) Le = 80

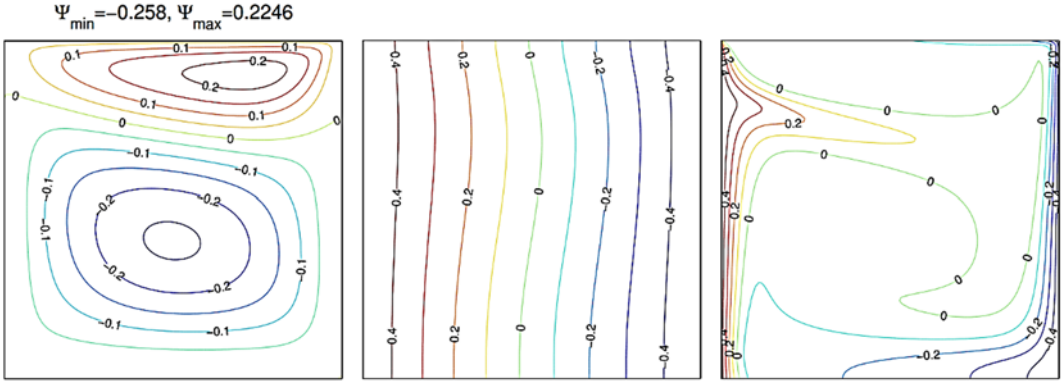

(d) Le = 200

(e) Fig. 5. Streamlines (left), isotherms (middle) and isoconcentrations (right) evolutions by varying the Lewis number for Da = 10^{-2}, M_{aT} = −100 and ε = 0.7.

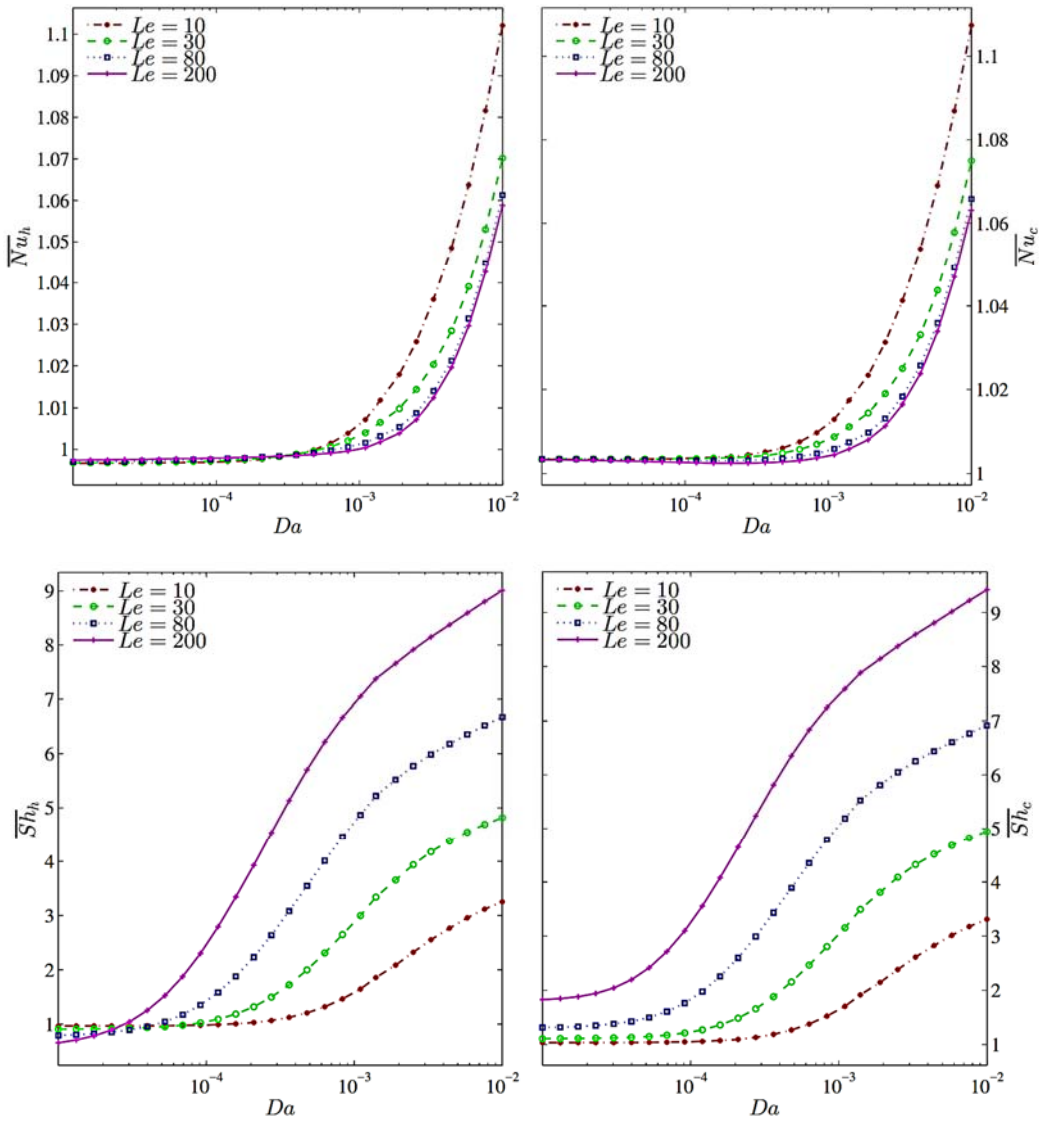

Fig. 6. Average Nusselt number (a) and Sherwood number (b) on the hot wall (left) and the cold wall (right) with Da for different Le at ε=0.7 and M_{aT}=−100.

of an asymptotic convection regime where the Nuh and Nuc are independent of the Darcy number for the four Lewis number. Careful investigation shows that the average Nusselt number remains constant up to Da = 8.3 × 10^{-4}. The average Nusselt number are observed identic for the different Le value. Later, the Nu is no longer identic, higher Lewis number gives lower Nu values. This due to as the Lewis numbers increases, the induced buoyancy forces, due to mass transfer effects, are strong, but the effective regions are very limited. The differences grow explicitly by increasing the Darcy number. Contrast to the Nu, the Sh increases with increasing the Lewis number for Da > 8.3 × 10^{-4}. The Shh and Shc values are almost equal for each Da. The onset of solutal diffusivity starts at lower Da for greater Le, but the onset of thermal convection starts at the same Da for the all Lewis number.

Variations of the average Nusselt number along the hot and cold walls with the Darcy number are shown in Fig. 7 (a) for different values of thermal Marangoni number M_{aT} at ε = 0.7 and Le =

10. In general, the heat transfer increases with increasing the Darcy number. This is due to the porous matrix become more permeable at larger Da that increasing flow intensity. The strongest counteracting surface tension gives the highest average Nusselt number along the hot wall, while the strongest augmenting surface tension gives the highest average Nusselt number along the cold wall for the considered Da. The Nuh and Nuc are almost constant by increasing the Darcy number for MaT = −100, 100. They also remains unchanged by changing the M_{aT} = −100 to M_{aT} = −100 for Da < 10^{-3}. It contrast to changing the M_{aT} =−1000 to M_{aT} = 1000 where the Nuc remains unchanged for Da > 10^{-3}. Similar to the Nu, the Sh increases with increasing the Darcy number. The strongest counteracting surface tension gives the highest average Sherwood number along the hot wall for all Da, but it gives the lowest Sh in range Da < 10^{-4}

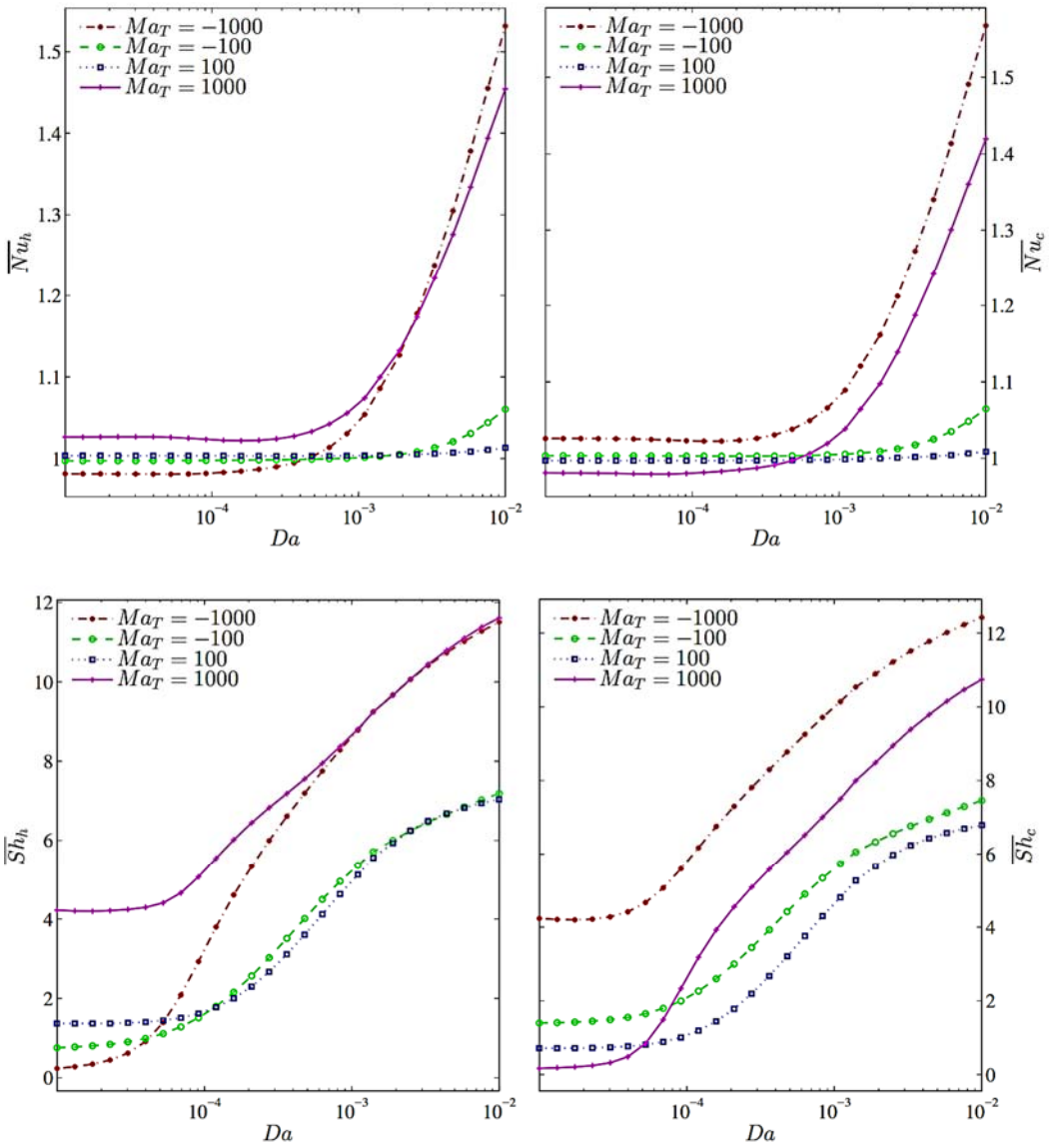

Fig. 7. Average Nusselt number (a) and Sherwood number (b) on the hot wall (left) and the cold wall (right) with Da for different M_{aT} at ε=0.7 and Le=10.

(Darcy regime) and the highest Sh in range Da > 10^{-3} (non-Darcy regime). From the Nu and Sh profiles in the Fig. 7 also observes that the presence of the thermocapillary force effects at the non-Darcy regime had greater influence than those at the Darcy regime.

Figure 8 (a) shows the average Nusselt number along the hot and cold walls against the Marangoni number for different porosities at Le = 10 and Da = 0.01. As shown in the figure, the Ma varies from -1000 to 1000. The Nuh and Nuc decreases by reducing the counteracting surface tension force and increases by augmenting the surface tension force. In general, increasing the porosities increases the Nuh and Nuc for the considered M_{aT} . This is due to low porosity means more resistance to fluid flow. It observed that the insignificant effect of changing the porous medium porosities were obtained about $M_{aT} = -90$. This location also presents the minimum values of the both Nusselt number. The Sher-wood numbers is also showed minimum about the $M_{aT} = -90$ as displayed in Fig. 8 (b).Similar to the $\overline{Nu}$, the $\overline{Sh_h}$ and $\overline{Sh_c}$ decreases by reducing the counteracting surface tension force and increases by augmenting the surface tension force. This happen because the heat transfer rate and mass transfer rate are enforcing for the augmenting case, but both rates are suppressed by the local flow direction opposite to the main flow direction for the counteracting case.

5. CONCLUSIONS

The present numerical simulation study the double-diffusive natural and Marangoni convection in a porous cavity. The dimensionless forms of the governing equations are modelled and solved using

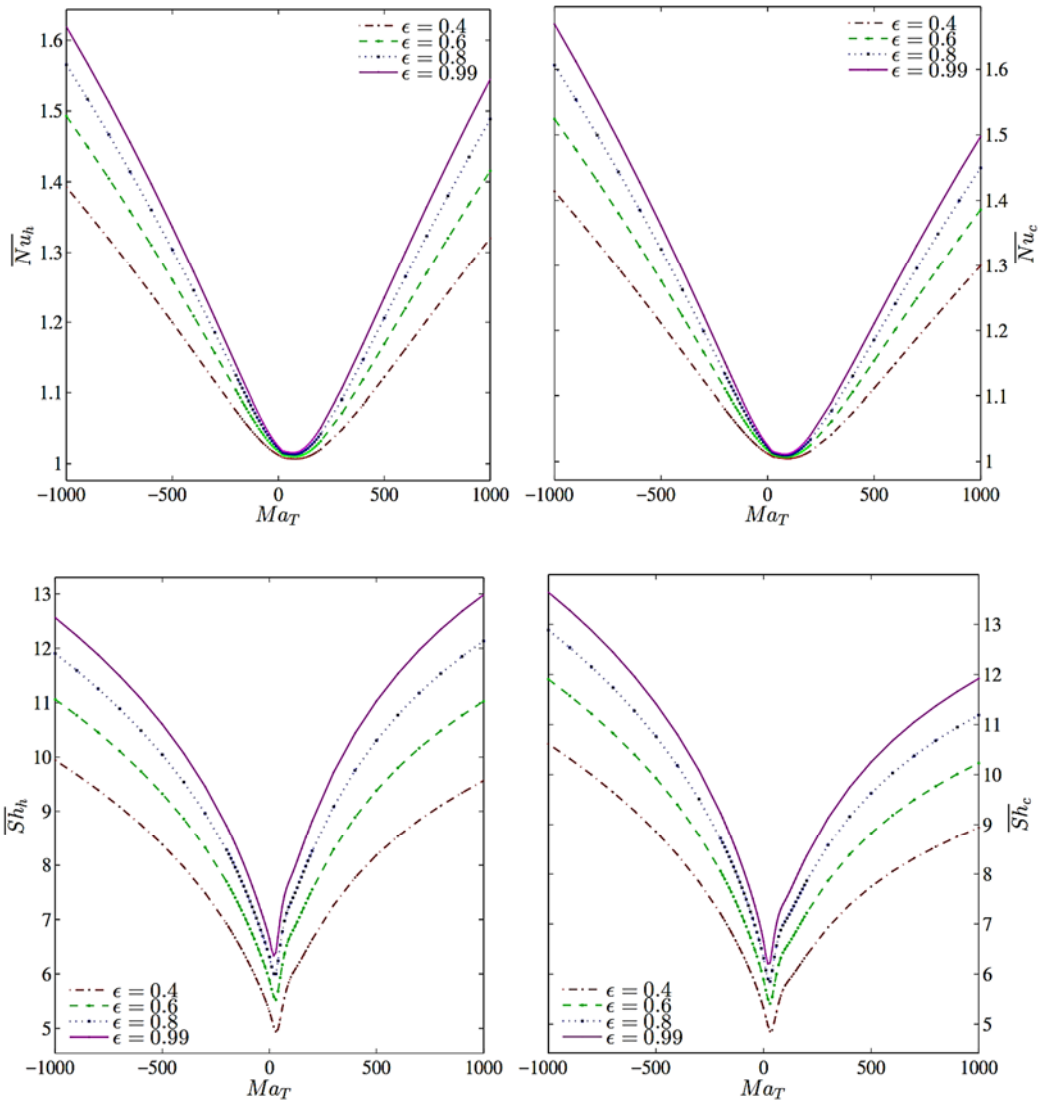

Fig. 8. Average Nusselt number (a) and Sherwood number (b) on the hot wall (left) and the cold wall (right) with Ma for different ε at Le=10 and Da=0.01.

the COMSOL program. Detailed computational results for flow, temperature and concentration field and the heat transfer rate in the cavity have been presented in the graphical form. The main conclusions of the present analysis are as follows:

1. The thermosolutal convection weakens while Marangoni convection strengthens by increasing the Lewis and Darcy numbers. The presence of the Marangoni forces effects at the non-Darcy regime had greater influence than those at the Darcy regime.
2. The performance between the global heat and solute transfer is significantly varied at relative small thermocapillary force effects.
3. The global heat and solute transfer rate decreases by reducing the counteracting surface tension force and increases by augmenting the surface tension force. The minimum values of the global heat and solute transfer rate were obtained about MaT = −90 for the all porosities.

CONFLICT OF INTERESTS

The authors declare there is no conflict of interests regarding the publication of this paper.

REFERENCES

Al-Farhany, K. and A. Turan (2012). Numerical study of double diffusive natural convective heat and mass transfer in an inclined rectangular cavity filled with porous medium. *Int. Comm. Heat Mass Transf. 39*, 174–181.

Arafune, K. and A. Hirata (1998). Interactive solutal and thermal marangoni convection in a rectangular open boat. *Numer. Heat Transf. Part A 34*, 421–429.

Arbin, N., H. Saleh, I. Hashim and A. Chamkha

(2016). Numerical investigation of double–diffusive convection in an open cavity with partially heated wall via heatline approach. *Int. J. Thermal Sci. 100*, 169–184.

Benissaad, S. and N. Ouazaa (2012). Analytical and numerical study of double diffusive natural convection in a confined porous medium subjected to heat and mass fluxes. *J. Porous Media 15*, 909–926.

Bergman, T. L. and S. Ramadhyani (1986). Combined buoyancy- and thermocapillary-driven convection in open square cavities. *Numerical heat transfer 9*, 441–451.

Carpenter, B. M. and G. M. Homsy (1989). Combined buoyant-thermocapillary flow in a cavity. *J. Fluid Mech. 207*, 121–132.

Chamkha, A. (2002). Double-diffusive convection in a porous enclosure with cooperating temperature and concentration gradients and heat generation or absorption effects. *Numer. Heat Transf. Part A 41*, 65–87.

Ergun, S. (1952). Fluid flow through packed columns. *Chem. Eng. Prog. 48*, 89–94.

Ghalambaz, M., F. Moattar, M. A. Sheremet and I. Pop (2016). Triple-diffusive natural convection in a square porous cavity. *Transp. Porous Med. 111*, 59–79.

Goyeau, B., J. P. Songbe and D. Gobin (1996). Numerical study of double-diffusive natural convection in a porous cavity using the Darcy-Brinkman formulation. *Int. J. Heat Mass Transf. 39*, 1363–1378.

Hadid, H. B. and B. Roux (1992). Buoyancy and thermocapillary-driven flows in differentially heated cavities for low-prandtl number fluids. *J. Fluid Mech. 235*, 1–36.

Hadidi, N., R. Bennacer, and Y. Ouldamer (2016). Numerical study of double-diffusive convection developed within horizontal partially porous enclosure. *Desalination and Water Treatment 0*, 1–8.

Hossain, M. A., M. Z. Hafiz, and D. A. S. Rees (2005). Buoyancy and thermocapillary driven convection flow of an electrically conducting fluid in an enclosure with heat generation. *Int. J. Thermal Sci. 44*, 676–684.

Jue, T. C. (1998). Numerical analysis of thermosolutal marangoni and natural convection flows. *Numer. Heat Transf. Part A 34*, 633–652.

Karimi-Fard, M., M. Charrier-Mojtabi and K. Vafai (1997). Non-Darcian effects on double-diffusive convection within a porous medium. *Numer. Heat Transf. Part A 31*, 837–852.

Liu, D., F. Y. Zhao and G. F. Tang (2008). Thermosolutal convection in saturated porous en-closure with concentrated energy and solute sources. *Energy Conversion and Management 49,* 16–31.

Mamou, M., P. Vasseur and E. Bilgen (1995). Multiple solutions for double-diffusive convection in a vertical porous enclosure. *Int. J. Heat Mass Transf. 38*, 1787–1798.

Nithiarasu, P., K. Seetharamu and T. Sun dararajan (1985). Natural convection with combined heat and mass transfer buoyancy effects in a porous medium. *Int. J. Heat Mass Transf. 28*, 1597–1611.

Nithiarasu, P., K. Seetharamu and T. Sundararajan (1996). Double-diffusive natural convection in an enclosure filled with fluid-saturated porous medium: a generalized non-Darcy approach. *Numer. Heat Transf. Part A 30*, 413–426.

Rudraiah, N., M. Venkatachalappa and C. K. Subbaraya (1995). Combined surface tension and buoyancy-driven convection in a rectangular open cavity in the presence of a magnetic field. *Int. J. Non-Linear Mech. 30*, 759–770.

Saleem, M., M. A. Hossain, S. Mahmud and I. Pop (2011). Entropy generation in Marangoni convection flow of heated fluid in an open ended cavity. *Int. J. Heat Mass Transf. 54*, 4473–4484.

Srinivasan, J. and B. Basu (1986). A numerical study of thermocapillary flow in a rectangular cavity during laser melting. *Int. J. Heat Mass Transf. 29*, 563–572.

Strani, M., R. Piva and G. Graziani (1983). Thermocapillary convection in a rectangular cavity: asymptotic theory and numerical simulation. *J. Fluid Mech. 130*, 347–376.

Tofaneli, L. A. and M. J. S. de Lemos (2009). Double-diffusive turbulent natural convection in a porous square cavity with opposing temperature and concentration gradients. *Int. Comm. Heat Mass Transf. 36*, 991–995.